journal

J. Am. Ceram. Soc., 77 [8] 2025–35 (1994)

Plasticity-Induced Fatigue Damage in Ceria-Stabilized Tetragonal Zirconia Polycrystals

Shih-Yu Liu* and I-Wei Chen*

Department of Materials Science and Engineering, The University of Michigan, Ann Arbor, Michigan 48109-2136

Current studies on the fatigue lifetime of ceramics are mostly focused on the relation between the stress amplitude (or maximum stress) and cycles to failure. For a more compliant and plastic ceramic which has a pronounced nonlinear stress–strain relation, the role of plastic strain in the fatigue damage is investigated for the first time in this study using a 12 mol% Ce-TZP. By testing at different temperatures, we were able to vary the amount of transformation plasticity with the same microstructure. The Coffin–Manson relationship, which suggests that fatigue lifetime in the low cycle fatigue regime is best correlated with the plastic strain range, was confirmed for the tough ceramic. Fatigue damage is found to be a bulk process which continuously degrades flaw tolerance by microcracking. Evidence for the latter mechanism was also provided by uniaxial cyclic tension–compression stress–strain response and by TEM examination. Despite such damage, the possibility of plasticity-induced surface-crack nucleation in fatiguing ceramics, unlike in metals, appears unimportant.

I. Introduction

In the fatigue literature of metals, fatigue lifetime is customarily divided into two regimes (high cycle fatigue and low cycle fatigue) according to their relationship with the cyclic strain range.[1] In the high cycle fatigue regime, in which the maximum cyclic stress lies below or around the yield stress level, fatigue lifetime is controlled by the cyclic *elastic* strain range. On the other hand, when the material is stressed into a higher level with extensive plastic deformation, i.e., in the low cycle regime, fatigue lifetime is better correlated with the *plastic* strain range. This distinction has not been made in the studies of ceramic materials in the past because of the very limited plastic deformation available in all the ceramics studied.[2–20] It was generally assumed that stress (either the stress amplitude or maximum stress) was the controlling parameter for fatigue lifetime and the plastic strain range was considered too small and too impractical to be a correlation parameter. Although the above approach seems reasonable for brittle ceramics, caution is needed in dealing with toughened ceramics which derive a very pronounced contribution to toughness from plastic deformation. To critically examine this issue, we have compared ceramics of identical microstructure and elastic properties but with different plastic response using ceria-stabilized tetragonal zirconia polycrystals (Ce-TZP). Plasticity in Ce-TZP has its origin in phase transformation.[21,22] Lowering the test temperature without changing the microstructure increases the driving force for the phase transformation, which in turn results in a higher amount of transformation plasticity. Compared to the other two zirconia materials which were studied previously, yttria-stabilized zirconia (Y-TZP)[23–25] and magnesia-stabilized zirconia (Mg-PSZ),[25] Ce-TZP is notable in that its plasticity can be much greater in magnitude.[26] This makes Ce-TZP an ideal ceramic material to investigate the plastic strain effect on fatigue.

Inasmuch as plasticity-dominated fatigue behavior might be expected in Ce-TZP, it is also interesting to question the relevance of fatigue crack nucleation by deformation, especially in the near surface regions. Current understanding of fatigue behavior in metals and polymers states that the fatigue lifetime is a three-stage process including initiation, propagation, and final failure, and that a large plastic strain range facilitates

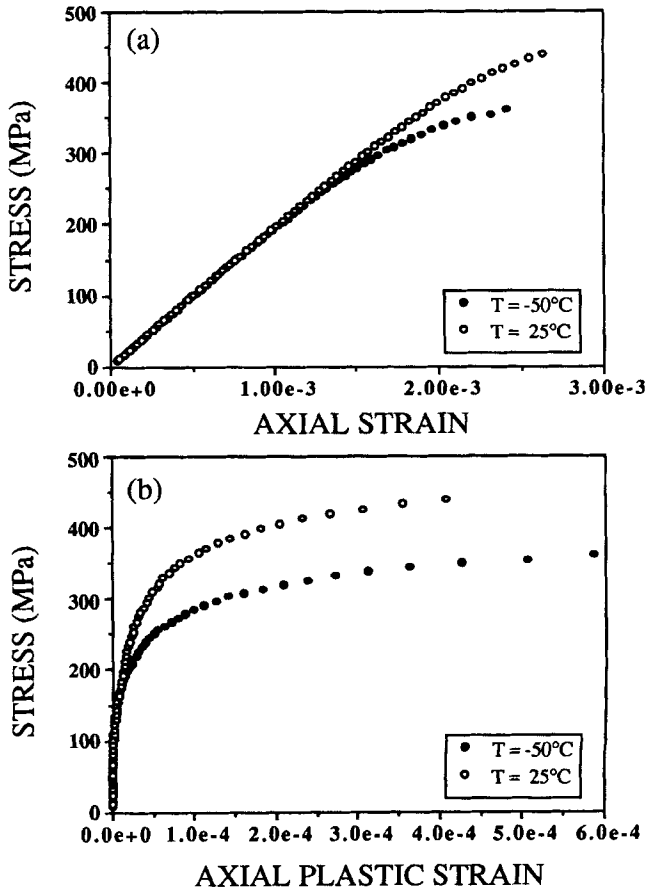

Fig. 1. (a) Stress–strain and (b) stress–plastic strain curves of Ce-TZP in tension tests at −50° and 25°C.

G. Grathwohl—contributing editor

Manuscript No. 194327. Received August 4, 1993; approved April 29, 1994.
Presented at the 94th Annual Meeting of the American Ceramic Society, Minneapolis, MN, April 15, 1992 (Paper No. 10-IXI-92).
Supported by the U.S. National Science Foundation under Grant No. DMR-9119598.
*Member, American Ceramic Society.

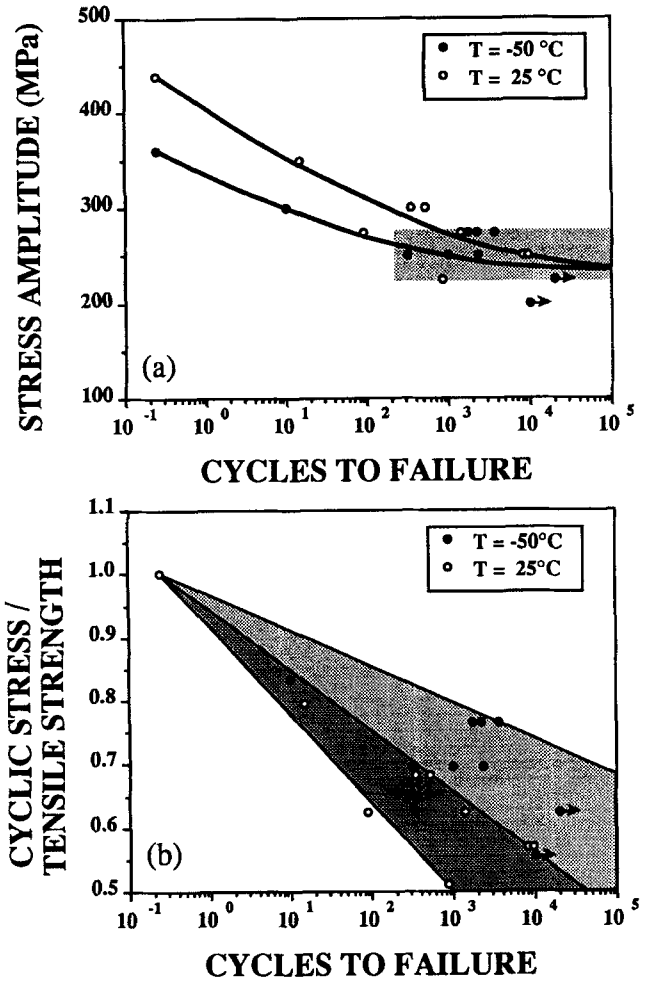

Fig. 2. (a) Stress amplitude and (b) stress amplitude normalized by the tensile strength vs failure cycle curves of Ce-TZP at −50° and 25°C.

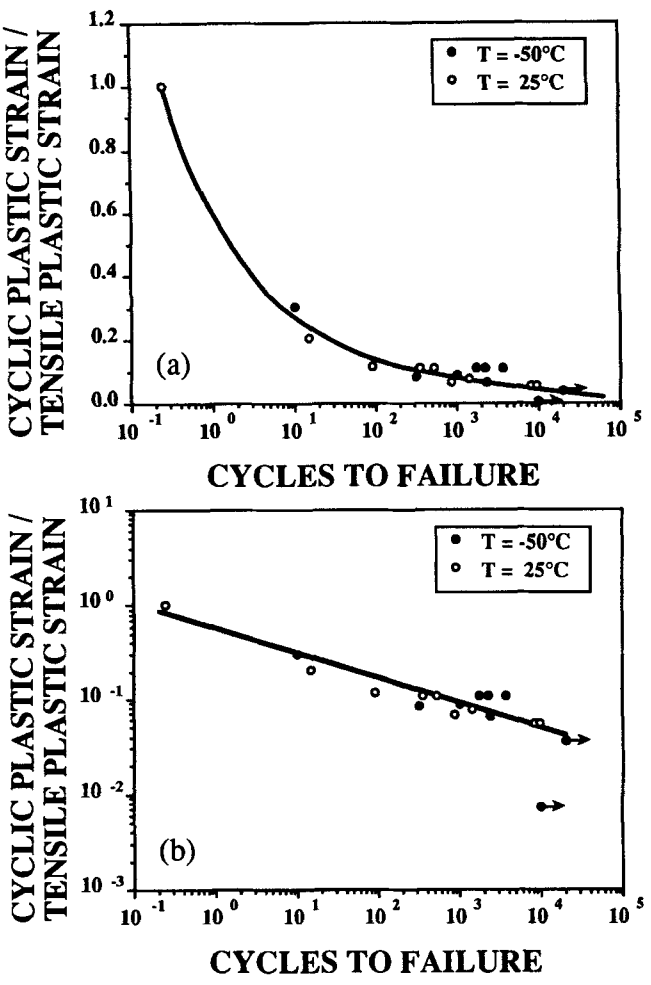

Fig. 3. Plastic strain range normalized by the tensile plastic strain vs cycles to failure in the (a) semilog and (b) log–log scale.

immediate crack nucleation at the specimen surface.[1] Although our previous study of Y-TZP found that the fatigue life was entirely controlled by the propagation of preexisting flaws and that no evidence of crack nucleation could be detected, a more general resolution of this issue must await an evaluation of more plastic ceramics.[23,24] Ce-TZP, with its unusually large transformation plasticity, is quite flaw tolerant, having a Weibull modulus in the range of 40[27] and very little tendency for crack initiation even under heavy damage such as indentation. It is thus interesting to see whether in this ceramic preexisting flaws cease to dominate fatigue life and surface crack nucleation becomes important.

II. Experimental Procedure

(1) Material

Ce-TZP powder, having a nominal composition of 12.5 mol% ceria and 87.5 mol% zirconia, was obtained from a commercial source (Tosoh Corp., New Milford, CT). The as-received powder was first compacted inside a rubber die, then cold isostatically pressed at 200 MPa. The green compacts, with a diameter of 20 mm and a length of 120 mm, were sintered in air at 1600°C for 8 h. The sintered material has a density of 6.24 g/cm^3 and contains primarily a tetragonal phase (95%) plus a small fraction of monoclinic phase. Test specimens were machined by grinding using a 220-grit diamond wheel to have a 16-mm gauge length and a 6-mm gauge diameter that conform to ASTM E606.[28] Some specimens were also machined into an hour-glass shape with a radius of 100 mm to provide a modest stress gradient for the observation of surface nucleation. In all cases, a large amount of material around the gauge section was removed by machining so that any surface

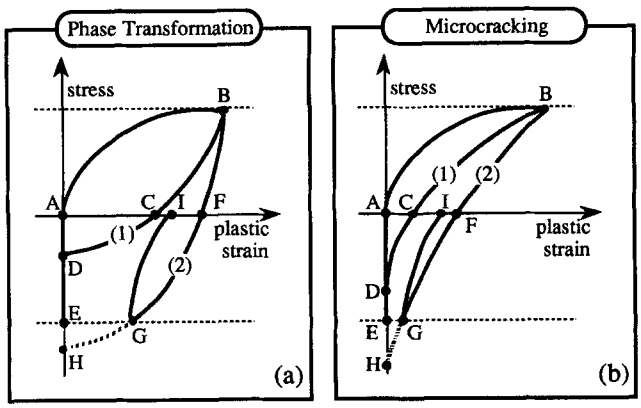

Fig. 4. (a) Transformation and (b) microcracking-induced hysteresis loops in zirconia-containing ceramics.

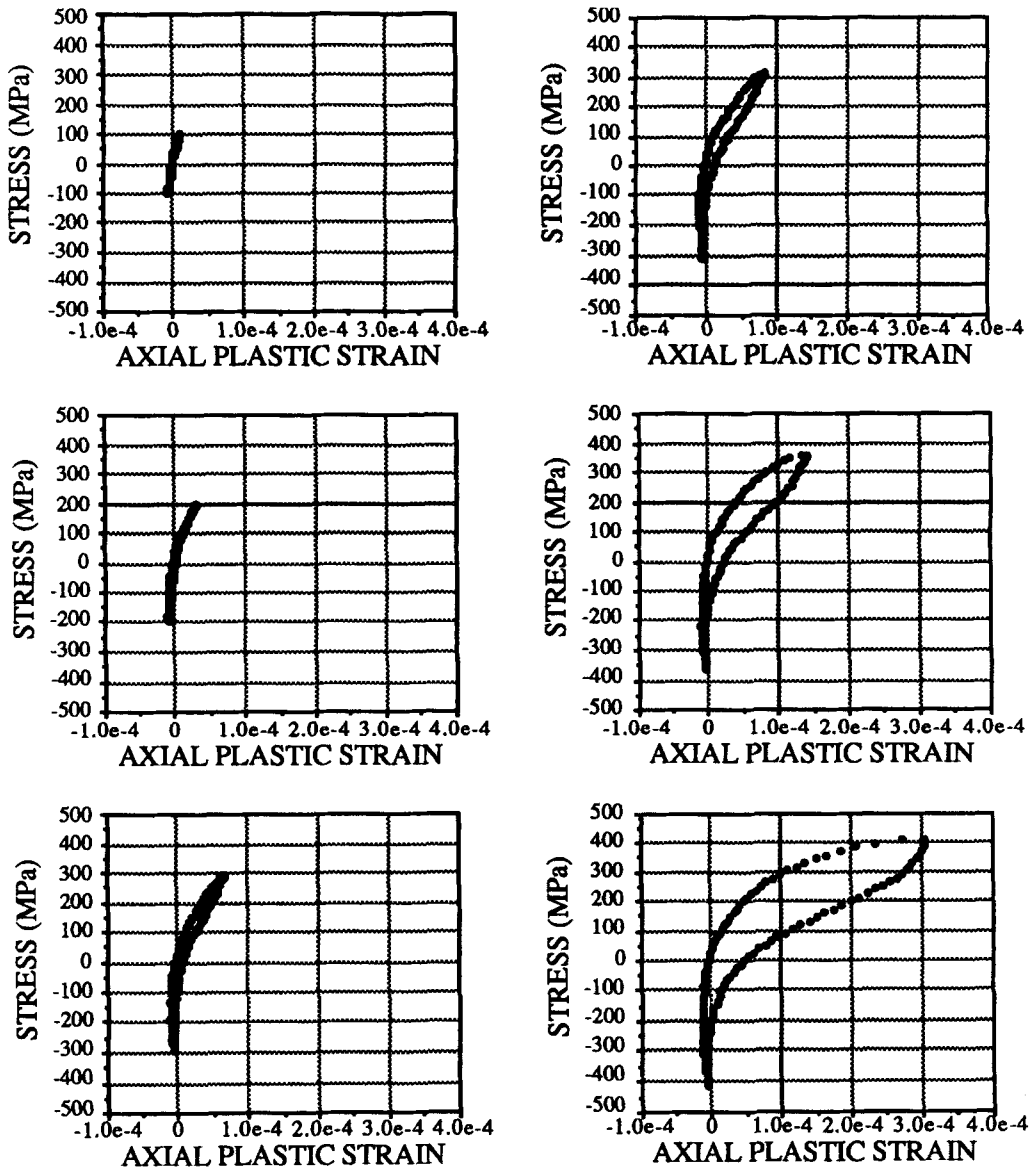

Fig. 5. Axial hysteresis loops of Ce-TZP at 25°C.

inhomogeneities introduced during sintering would not remain. A final mirror surface finish was obtained by polishing with 1-μm-diamond paste.

The sintered material was first tested to find out the tetragonal to monoclinic transformation temperature. A burstlike volumetric dilation that signaled the phase transformation was detected at −130°C. This material was also examined under a microscope to reveal a relatively uniform microstructure with a grain size of 8 μm. Finally, after machining, a 2-h annealing at 1000°C was performed to remove any surface residual stress before fatigue testing.

(2) Fatigue Testing

Load-controlled, fully reversed, uniaxial low cycle fatigue tests were conducted using a computer-controlled servo-hydraulic testing machine (MTS 810, MTS Systems Corp., Minneapolis, MN) with a load capacity of 100 kN. An axial extensometer having a gauge length of 8 mm was attached to the central portion of the specimen by two springs. In some cases, a diametral extensometer was also used to simultaneously record the radial strain. Both extensometers provided an accuracy better than 10^{-5} for the strain measurements. Before fatigue testing, a dye was applied to the specimen surface and dried by overnight baking to reveal any preexisting surface damage. Fatigue tests were conducted at ambient (25°C) and low temperature (−50°C) to produce different amounts of transformation plasticity. A sinusoidal cyclic stress wave form was used at a frequency of 5 Hz. Fracture surfaces of specimens were examined by scanning electron microscopy to reveal fracture origins and other notable features.

(3) Microscopy

Standard light microscopy and scanning electron microscopy (SEM) were performed for the tested materials to examine their microstructure and fracture-related features. In addition, transmission electron microscopy (TEM) was used to reveal microcracks in the tested specimens. The TEM specimens in the form of thin disks were cut from regions close to the fracture surface. They were perpendicular to the fracture surface in view of the likely orientation of transverse microcracks. These disks were thinned by standard procedure and examined using a Philips 430 electron microscope operating at 120 kV.

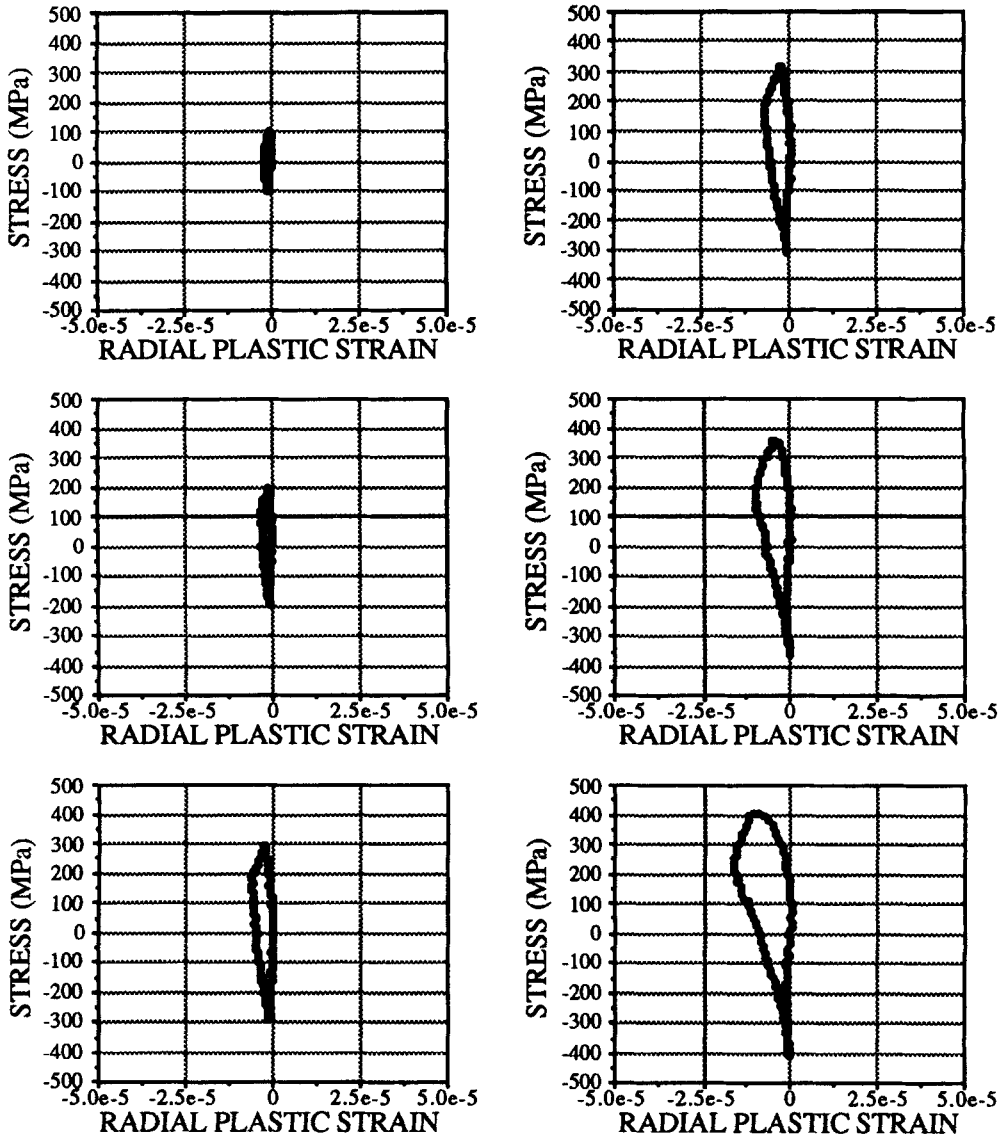

Fig. 6. Radial hysteresis loops of Ce-TZP at 25°C.

III. Results and Analysis

(1) Tensile Stress–Plastic Strain Curve

Tensile stress–strain curves of Ce-TZP tested at 25° and −50°C are shown in Fig. 1(a). Tensile strength and total strain to failure at 25°C were found to be greater than those at −50°C. However, the plastic strain of the specimen tested at the lower temperature was 30% greater. This contrast becomes more obvious when the stress is plotted against the plastic strain as shown in Fig. 1(b). (The plastic strain is obtained by subtracting the elastic portion, which is calculated from $\sigma/E_{apparent}$, from the total strain. Here σ is applied stress, and $E_{apparent}$ is the slope of the stress–strain curve between 0 and 50 MPa.) The reduction of the flow stress for plastic deformation may be attributed to the lower critical stress required to trigger the *t*-to-*m* phase transformation when the material is tested at a temperature closer to the *t*-to-*m* burst temperature.[21] More extensive transformation before failure is also apparent at −50°C, despite a lower ultimate tensile stress. At fracture the proportion of plastic strain in the total strain increases from 15% to 25%, when the test temperature decreases from 25° to −50°C.

(2) Stress–Life and Strain–Life Relationship

The cyclic stress–life (*S–N*) curves plotted in stress amplitude vs cycles to failure are shown in Fig. 2(a) for two test temperatures. The fatigue limits at 10000 cycles, below which fatigue failure is avoided, are around 225 MPa at both test temperatures. However, data scatter in this regime is quite large. Therefore, a definite fatigue limit cannot be identified, and test data of the two temperatures appear to fall into the same broad band. At higher stress levels, about 300 MPa, the fatigue lifetimes increase with test temperature. For example, at a stress amplitude of 300 MPa, specimens tested at 25°C survived up to 500 cycles, while the one tested at −50°C failed within 10 cycles.

The different fatigue lifetimes at two temperatures cannot be accounted for by the difference in the tensile strength alone. If the stress amplitude is normalized by tensile strength as shown in Fig. 2(b), the data of the two temperatures still fall into two distinct bands. On the other hand, the different fatigue lifetimes correlate well with the different plastic strains. This is shown by replotting the data versus strain range, which is itself normalized by the tensile plastic strain as in Fig. 3(a). It is seen that, in such a plot, data at both temperatures fall on the same curve. Furthermore, on a log–log scale, as shown in Fig. 3(b), a linear relationship between the plastic strain range and cycles to failure—the so-called Coffin–Manson relationship—can be

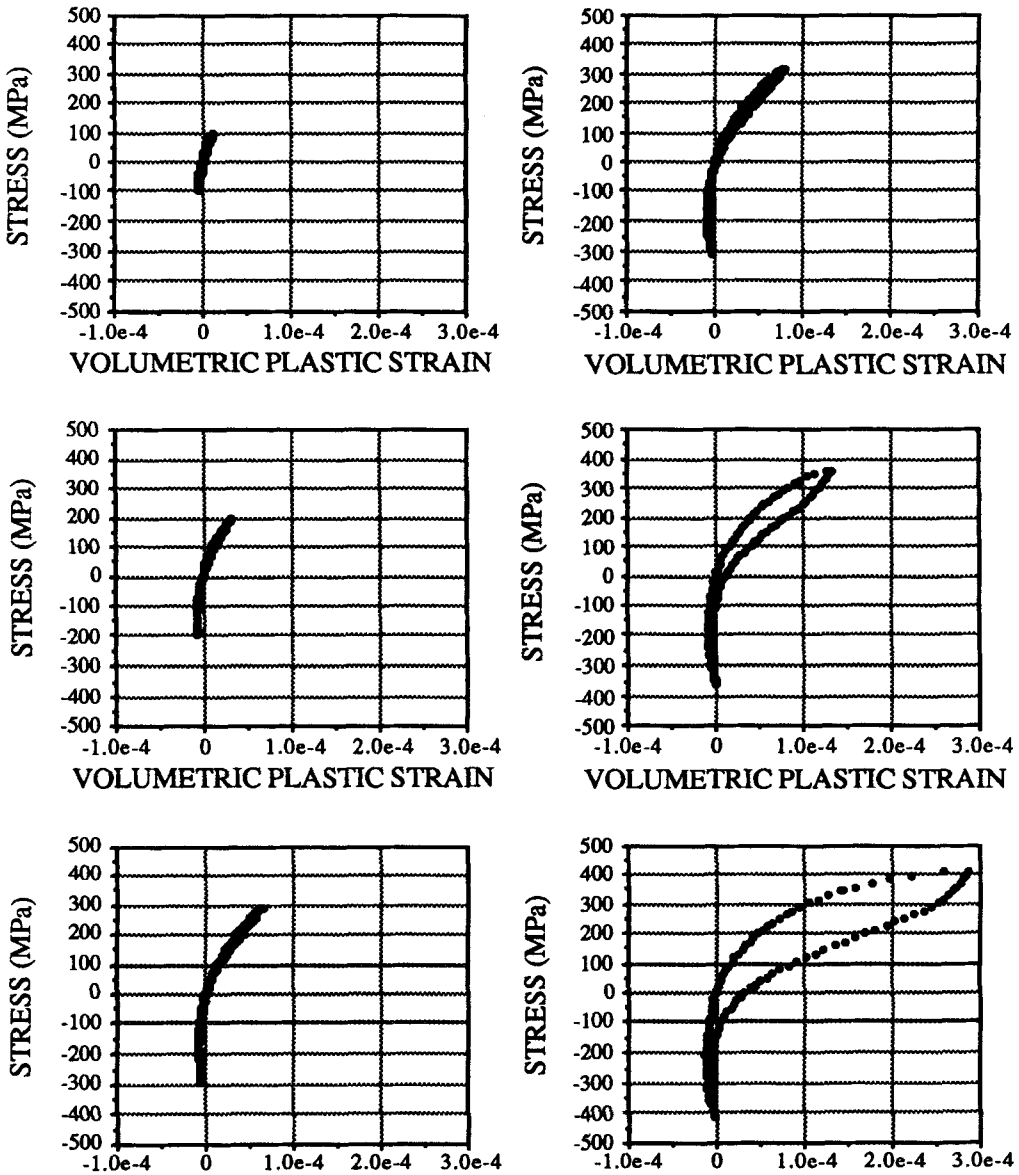

Fig. 7. Volumetric hysteresis loops of Ce-TZP at 25°C.

readily recognized. Thus, it is clear that the proportion of the plastic strain range to the tensile plastic strain is the only life-determining parameter.

(3) Hysteresis Loop

Before we present our results on hysteresis loops, it is instructive to briefly review the two types of hysteresis loops expected for transformation-toughened ceramics (see Figs. 4(a) and (b)).[25] When the transformation strain is dominant, the hysteresis loop (Fig. 4(a)) contains a portion AB representing the forward transformation plasticity. During unloading, the reverse phase transformation is represented by BCD. Here we assume the forward phase transformation is not fully reversed at zero stress but is at point D, below which only elastic compression continues (DE). (Since phase transformation in zirconia has a much higher yield stress in compression than in tension,[21,22] we may assume that no negative plastic strain representing further transformation assisted by the compression takes place.) Unloading from the peak compressive stress is then elastic (EA) and completes the first cycle. For the case in which forward phase transformation is not fully reversed even with load reversal, the tensile unloading curve follows BFGI and results in a finite residual plastic strain (AI) and an open loop. The salient feature of these loops when transformation strains dominate is the *positive* unloading curvature. This is similar to the observations in metals where dislocation plasticity dominates and a positive curvature is always associated with the unloading curve.

In the case of microcracking dominance (Fig. 4(b)), the portion AB is due to microcrack formation and opening, which relieves residual stresses and increases some elastic compliance. During unloading, some crack face contacts start to form and to bear load. This results in a stiffness recovery (through BCD) until all the cracks are closed (point D). Below that, a vertical portion also appears (DE) indicating elastic compression. If the full closure of microcracks cannot be completed before load reversal, then the unloading curve will follow BFGI and result in an open hysteresis loop. The common feature of these hysteresis loops when microcracking dominates is the *negative* unloading curvature, which is just the opposite of that in phase transformation. These two possibilities, transformation plasticity and microcracking, have been previously established by us to be the dominant deformation mechanisms in zirconia ceramics under cycling.[23,25]

A series of axial hysteresis loops of the first loading cycle, at 25°C and a stress rate of 20 MPa/s but at different stress ranges, is shown in Fig. 5. A positive curvature associated with the initial unloading portion is noted for all the axial hysteresis loops,

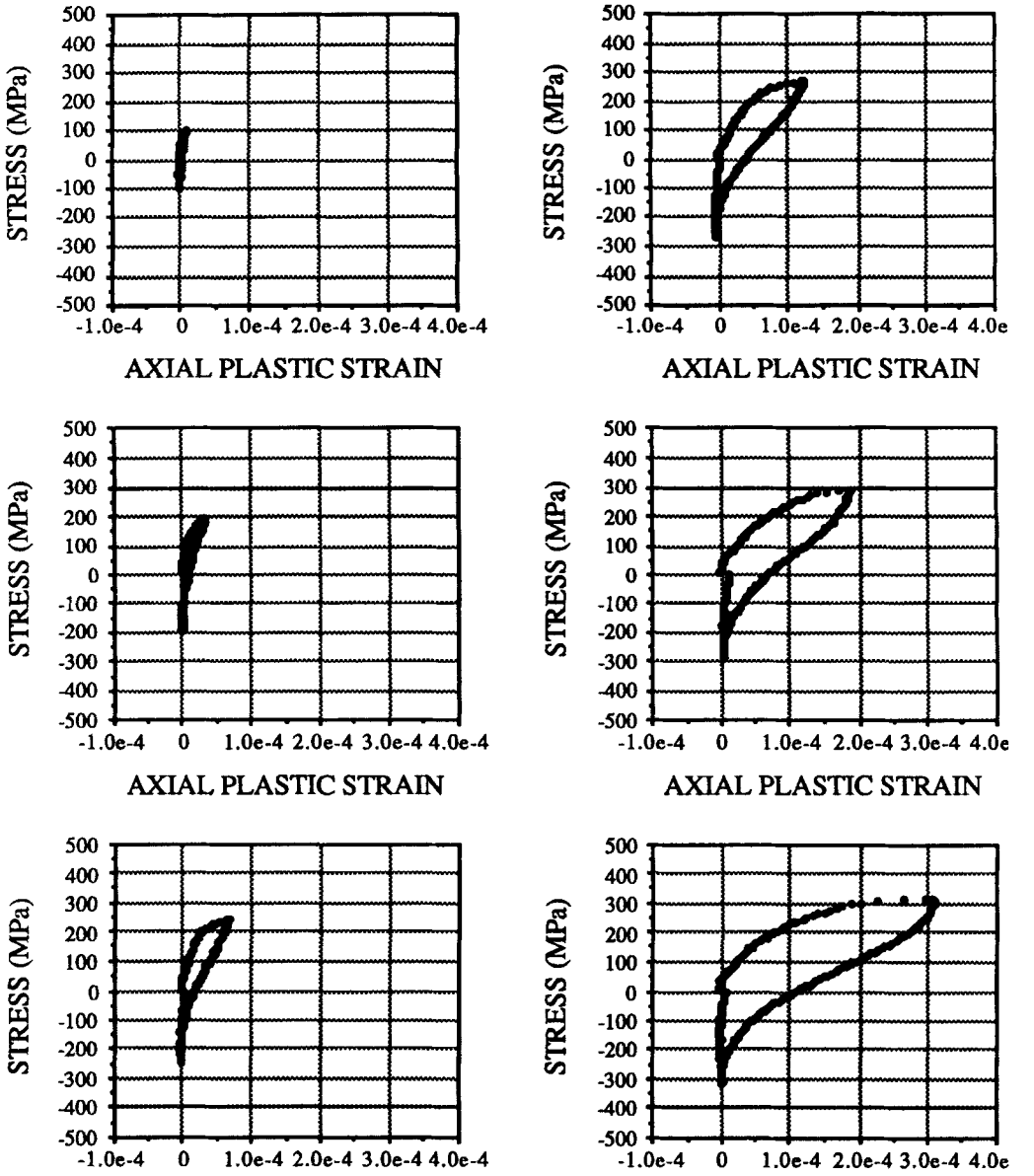

Fig. 8. Axial hysteresis loops of Ce-TZP at −50°C.

and it becomes especially prominent at higher stresses. This feature is most likely an indication of the dominance of transformation plasticity and not microcracking. Further unloading causes a positive-to-negative transition in curvature which could indicate the closure of microcracks. In the compressive half cycle, the slope of the stress–plastic strain curve continuously increases and approaches vertical, indicating the full closure of microcracks followed by pure elastic deformation at large compressive stresses. Unloading from the peak compressive stress causes the stress–plastic strain curve to retrace a nearly vertical line. If we take the inflection point of the unloading curve as the transition of dominant deformation mechanisms from transformation to microcrack closure, this seems to take place between 150 and 200 MPa for all hysteresis loops and seems to increase somewhat with the stress amplitude. Almost no plastic strain remains after the complete stress reversal and subsequent compression unloading; i.e., the hysteresis loops are closed. This seems to indicate that all forward transformation strain is reversed and that microcracks remain closed until a far-field tensile stress is applied.

The strain in the radial direction has also been simultaneously recorded and it is plotted against stress as shown in Fig. 6. Since microcracks induced during the tensile half cycle are probably preferentially aligned perpendicular to the loading axis, their contribution to the radial strain is minimal.[29] Thus, the radial hysteresis is primarily caused by phase transformation. A negative radial plastic strain was observed in the tensile loading cycle at all stress levels and increased in magnitude with increasing applied axial stress. (The negative sign is not surprising since transformation plasticity has a large shear component in addition to dilatation.[21,30]) During unloading the first part of the hysteresis curve acquires a positive slope, which must indicate a further net forward phase transformation despite the decreasing stress bias. Below a certain stress level, around 150 to 200 MPa, the slope turns negative for all the hysteresis loops, indicating a net reverse phase transformation. This transition seems to correspond to the inflection in the axial hysteresis loops shown in Fig. 5. The reverse phase transformation continues until a certain compressive stress level, below which only pure elastic deformation remains.

The lack of radial strain in compression provides direct evidence that no phase transformation in compression took place. This last point is also verified by constructing the volumetric hysteresis loops, which was obtained by summing axial hysteresis loops and twice the radial hysteresis loops. As shown in Fig. 7, there is no volume increase in the compression half

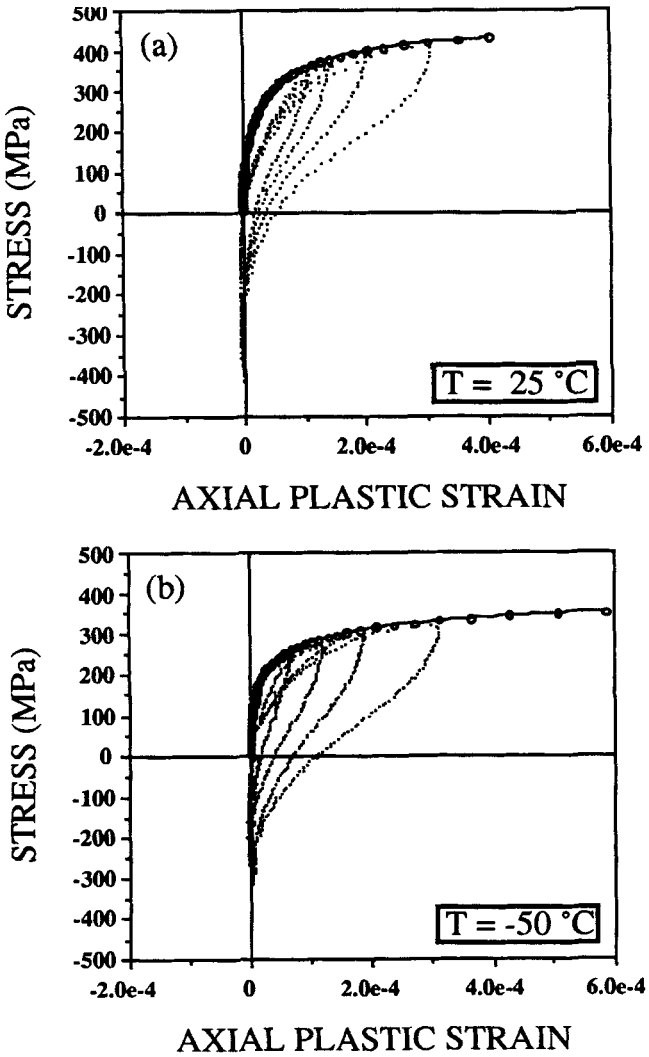

Fig. 9. Monotonic (open circles) and cyclic stress–plastic strain curves of Ce-TZP at (a) 25° and (b) −50°C.

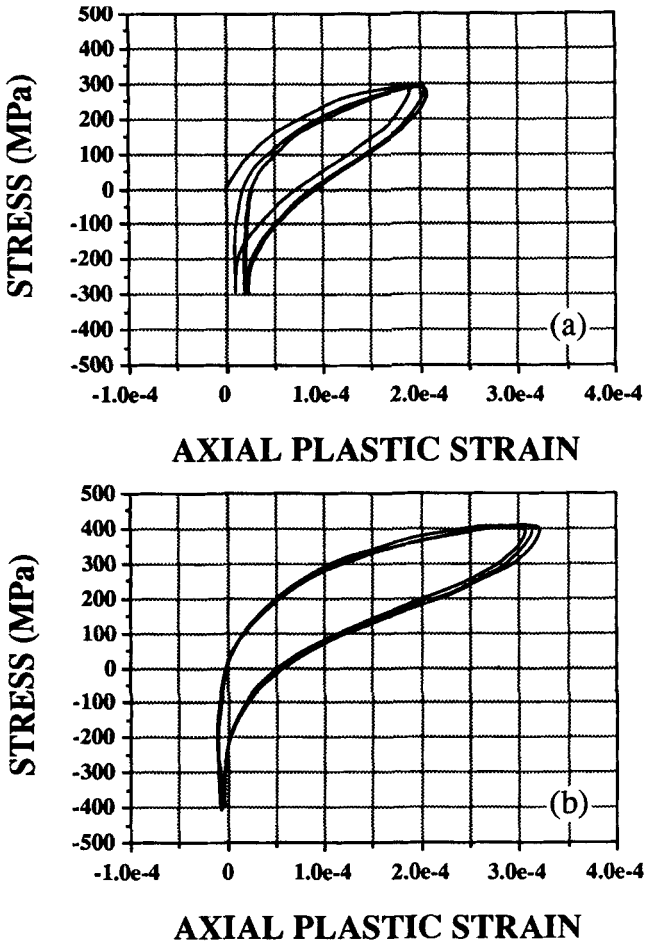

Fig. 10. Hysteresis loops showing cyclic softening (a) with accommodation and (b) without accommodation.

cycle. Other features of the volumetric hysteresis loops are similar to the axial hysteresis loops and are not further elaborated here.

A set of axial hysteresis loops obtained at −50°C is shown in Fig. 8 for comparison. They are similar to those obtained at 25°C (Fig. 5) but appear more flattened because of more pronounced plastic deformation at the lower test temperature. For example, the plastic strain at 325 MPa is about 3×10^{-4} at −50°C, while the plastic strain at the same stress level is less than 1×10^{-4} at 25°C. While the inflection points are now located at lower stresses. a negative curvature below that is evident and indicative of microcrack closure. Still, there is no transformation under peak compressive stress.

Cyclic stress–plastic strain curves at two testing temperatures are shown in Fig. 9. They were constructed by connecting the tips of the above first-cycle hysteresis loops at different stress amplitudes. These curves coincide with the monotonic stress–plastic strain curves of Fig. 1(b), which are also plotted in Fig. 9. This is not surprising because both sets of curves pertain to the first loading cycle. In fact, subsequent cycling does cause two types of cyclic softening, defined as an increase in the peak plastic strain and loop width. At a lower stress amplitude, cyclic deformation tends to accommodate itself and reaches a steady-state response during fatigue. In Fig. 10(a), the hysteresis loops of a specimen tested at −50°C show a finite residual strain after the first cycle but reach a steady-state response at the third cycle. This is characterized by the closure of the last hysteresis loop and the saturation of the peak plastic strain. On the other hand, at a higher stress level, cyclic deformation tends to accumulate progressively, leading to catastrophic failure. One such example is shown in Fig. 10(b), in which the peak plastic strain increases continuously. (Failure actually occurred in the fourth cycle. Note that data shown in Fig. 10 were obtained at a loading rate of 20 MPa/s rather than at a loading frequency of 5 Hz; therefore, they were not included in the fatigue lifetime curves shown in Figs. 2 and 3.)

(4) Fractography

A set of SEM micrographs taken from the circumference of a fatigue-fractured specimen tested at −50°C under ±250 MPa for 3653 cycles is shown in Fig. 11. Intergranular fracture with substantial crack branching can be clearly seen. Isolated surface cracks were found near the fracture surface, and they were evenly distributed all around the specimen. They were very localized, however, since no surface crack was traceable beyond 500 μm away from the fracture surface. In the hourglass-shaped specimen tested, we found failure to occur at a position some distance away from the waist section. (The stress level recorded though was not too different from that of the waist section, and the lifetime was within the range of normal scatter of our data.) Again, extensive crack branching and isolated surface cracks were found next to the main crack but not at the waist section.

Typical SEM micrographs taken from fatigue fracture surfaces are shown in Fig. 12. At both test temperatures long, hair-

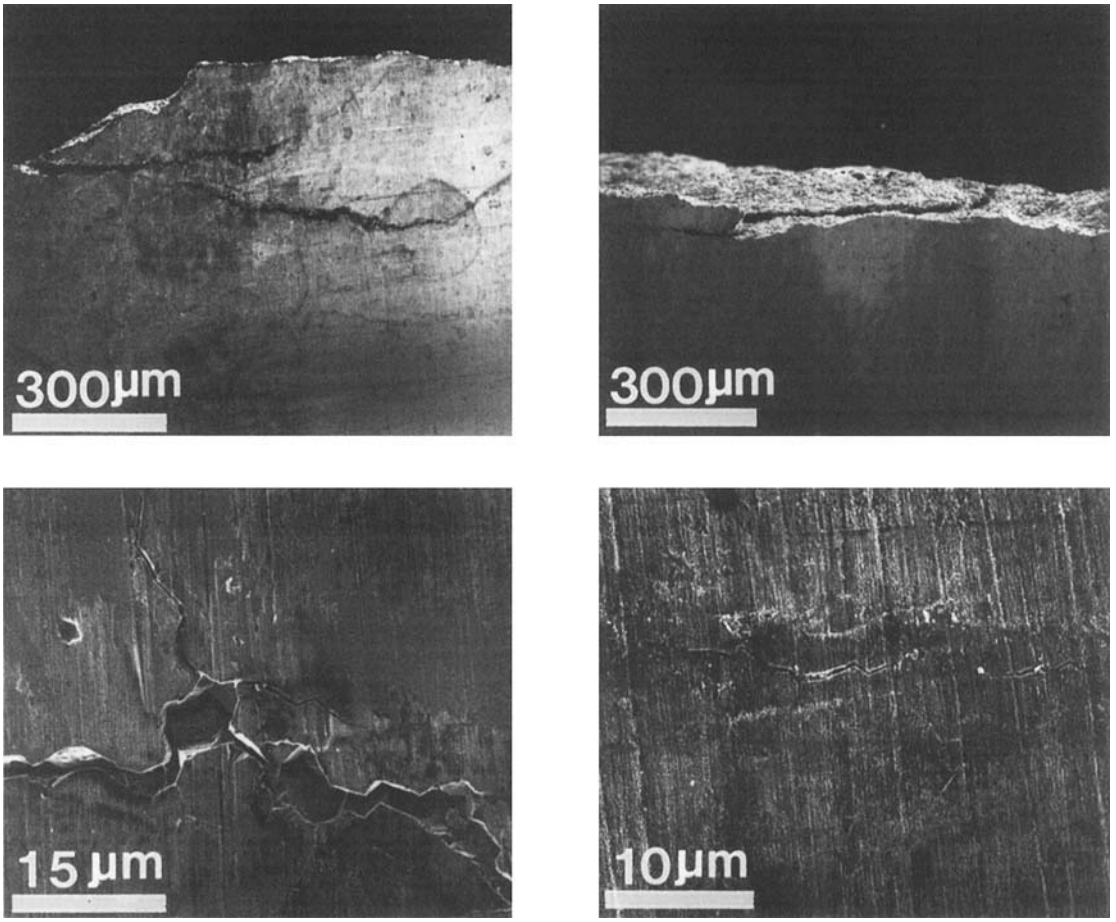

Fig. 11. SEM micrographs taken from the circumference of a fatigue-fractured specimen tested at −50°C, ±275 MPa for 3653 cycles.

line-like cracks connected to the free surface were identified as the fracture origins in most cases. The appearance of these fracture origins suggests that they were formed during processing and not during machining. The fracture features on samples tested at 25°C were essentially the same.

Fractography of monotonic overload fracture was also examined. Very similar features on both the fracture surface and the circumference were observed. These included extensive crack branching and isolated surface cracks on the circumference next to the main crack as well as the hairline fracture origins on the fracture surface.

Lastly, TEM examination of the regions near the fracture surface revealed a large number of microcracks which were situated on the grain boundaries. Several such examples are shown in Fig. 13. This specimen was taken from one tested at −50°C at σ_{max} = 275 MPa with a fatigue cycle of 2032. The examined region was approximately 3 mm from the fracture surface and was relatively thick in order to avoid artifacts caused by accidental cracking during specimen preparation and handling. Typically, the visible cracks were very sharp (thin) and often extended to the full length of a grain boundary. Linkage of microcracks was seldom observed in these specimens except between sintering pores.

IV. Discussion

(1) Plastic Strain-Controlled Fatigue Lifetime

For brittle ceramics, the common finding of a linear relationship between stress amplitude and failure cycles on a log–log scale has generally been rationalized by the continuous growth of the most critical preexisting flaw. The validity of this rationale relies on the existence of some sufficiently large processing flaws and a low flaw tolerance, so that any fatigue-nucleated crack has little probability of overtaking the larger preexisting flaws before final failure. It follows that the applied stress dictates the effective stress intensity at the crack tip and in turn determines the crack growth rate and hence the fatigue lifetime. Under these circumstances, fatigue degradation, other than the growth of the most critical preexisting flaw itself, is irrelevant to the fatigue lifetime. Indeed, plastic strain is most likely to be too small to be used as a correlation parameter.

Ce-TZP examined in this study apparently deviates from the above behavior in that it is the plastic strain amplitude that controls fatigue lifetime. Nevertheless, the fracture origins remain to be preexisting flaws and not those generated by cyclic plastic straining. (Evenly distributed, isolated surface cracks near the fracture surface were common to both monotonic and cyclic loading conditions and at both ambient and low temperatures. Hence, these surface cracks are believed to be associated with the final failure event and not with fatigue. In addition, surface cracks were found only next to the fracture surface in the hourglass specimen and not in the waist section, which had a slightly higher nominal stress. This also strongly suggests that it was preexisting flaws and not fatigue-nucleated damage which eventually caused fracture.) Thus, the plastic strain amplitude controls the fatigue lifetime, yet it is not responsible for the existence of the fatal flaw on the fracture surface. This apparent contradiction is unique to Ce-TZP and has not been noted previously in fatigue literature on metals.

The contradiction can be resolved if we envision the flaw tolerance of the material degrading in time with cyclic straining.

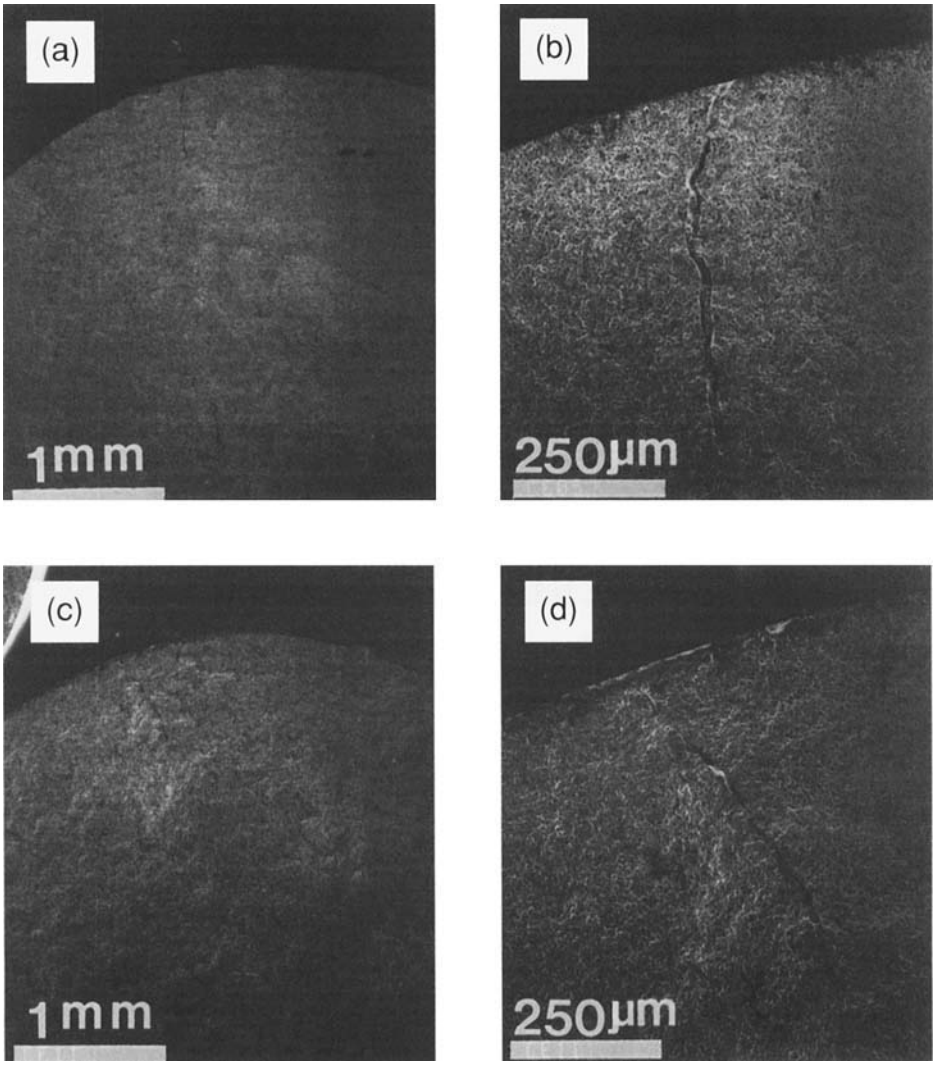

Fig. 12. Fracture origins of fatigue failure in Ce-TZP tested at (a,b) 25°C, ±300 MPa for 355 cycles and (c,d) −50°C, ±275 MPa for 2216 cycles.

As shown in Fig. 14(a), with pronounced transformation toughening, the growth of the largest preexisting flaw in Ce-TZP is initially retarded because of a rising R-curve. This would have led to a case of flaw tolerance even in fatigue in the virgin specimen. On the other hand, transformation plasticity triggered by cyclic plastic straining is capable of accumulating bulk damage in the form of microcracks.[29] Such damage is especially severe in Ce-TZP because of its capacity for large transformation strain.[26] (The presence of microcracks as a form of bulk damage is implicated by the shape of the hysteresis loop and further supported by the TEM observation of numerous microcracks situated on grain boundaries.) Although such microcracks are typically isolated from each other and thus not likely to form critical flaws directly responsible for fracture, they can reduce the toughness of the material, thereby facilitating the subsequent propagation of the preexisting flaws (Fig. 14(b)). In this way, we may picture fatigue lifetime in Ce-TZP to be mostly spent in the progressive degradation of damage tolerance, which is controlled by cyclic plastic straining, with the preexisting flaw becoming active (and critical in the end) only in the last part of the fatigue lifetime (Fig. 14(c)). (An alternative explanation of our observation relies on a strain-controlled crack growth mechanism. We are less disposed to the latter notion, however, in view of the intrinsic brittle nature of even a tough ceramic.) This picture is consistent with the observed behavior of Ce-TZP.

(2) Cyclic Deformation Mechanisms in Ce-TZP

The inflection point in the axial hysteresis loop and the returning point in the radial hysteresis loop mark the transition of the deformation mechanism from phase transformation to microcracking. This seems evident in Ce-TZP. The forward transformation is assisted by a tensile stress; therefore, it decreases rapidly with unloading. This can be most clearly seen on the radial strain curve that exhibits negative strain (due to transformation) only during initial unloading. Later, with transformation strain exhausted and with increasing stiffening due to crack closure, a negative curvature in the axial strain curve becomes manifest. In all cases, though, a compressive stress, which increases as the stress range increases, is required to restore the original volume (Fig. 7). Once this is achieved, the material is deformed elastically during further compressive loading and unloading. This is because no phase transformation in compression under a reasonable cyclic stress should take place; consequently no microcracking is triggered in compression either.

(3) Cyclic Deformation and Strain Irreversibility

In contrast to the results on Mg-PSZ in our previous study,[25] the closure of hysteresis loops was more readily achieved in Ce-TZP than in Mg-PSZ. This can be seen by comparing the hysteresis loops of Ce-TZP (Fig. 8) with those of Mg-PSZ (Figs. 13 and 14 in Ref. 25). The reason for the above finding

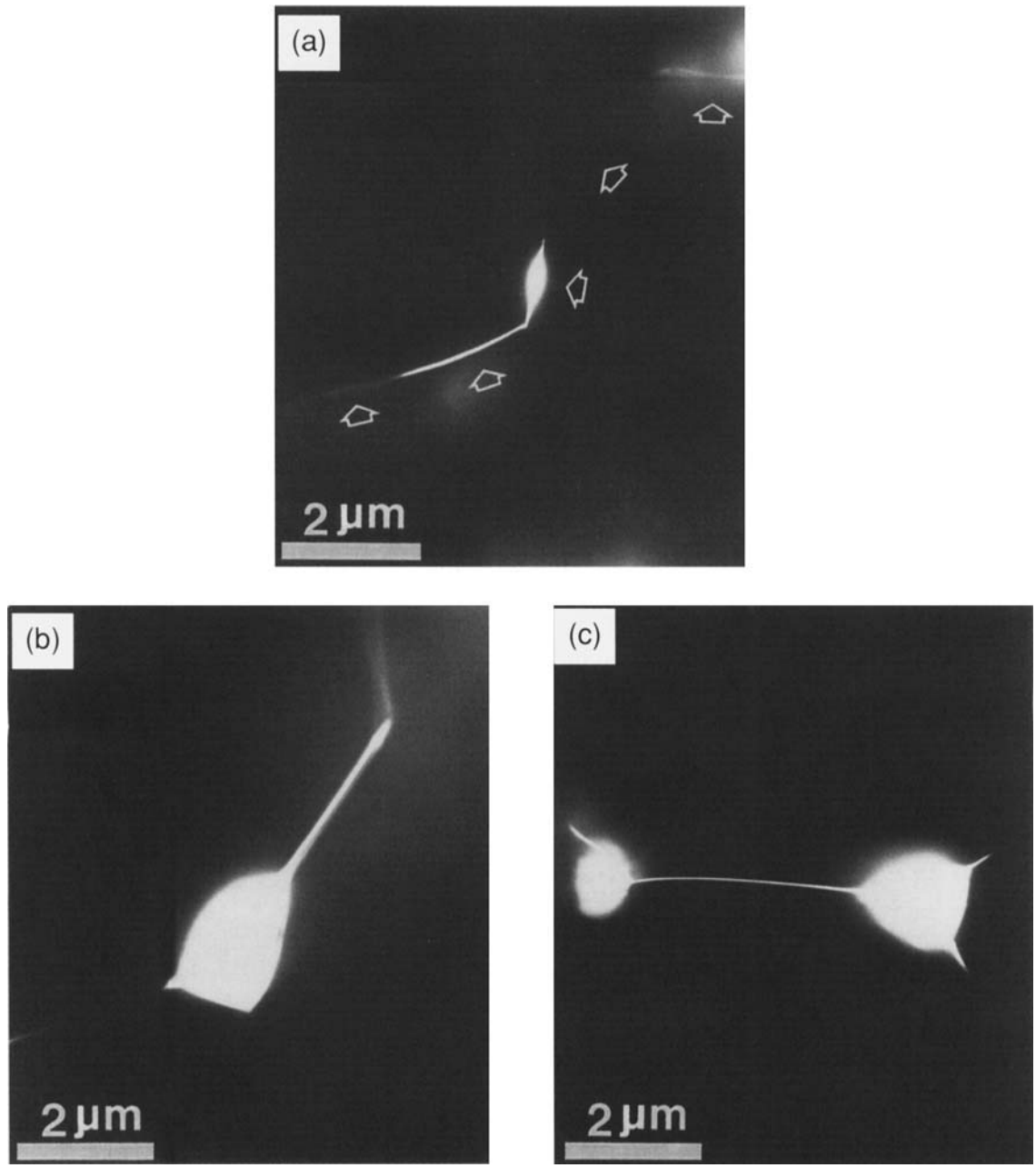

Fig. 13. TEM micrographs of Ce-TZP after fatigue show microcracks (a) along grain boundary, (b) extending from a sintering pore, and (c) linking between sintering pores.

may be related to their different microstructures, which are known to have important effects on the mode of transformation plasticity and the distribution of microcracks.[26,29] Chen *et al.* have shown experimentally and by thermoelastic considerations that smaller-grained materials have a lower temperature for monoclinic-to-tetragonal reversion.[22] Since transformation bands in Mg-PSZ tend to span across the entire grain,[30] despite the fact that tetragonal phase is in the form of precipitates dispersed in an inert matrix, their transformation should be less reversible than that in Ce-TZP because of the larger grain size. The other relevant consideration is the extent of microcracking that accompanies transformation. Transformation (strain) reversibility tends to decrease with increasing microcracking. This is because of the stress relief upon microcracking which removes the driving force for reverse transformation. According to the measurement of Chen *et al.*,[29] Mg-PSZ acquires more microcracking than Ce-TZP at the same amount of microscopic strain. It should be noted, however, that at large stress amplitudes, strain reversibility is progressively lost as evidenced by the increasing compressive stress required to restore the original volume (Fig. 7). Thus, despite a better strain reversibility, Ce-TZP is susceptible to fatigue when subject to a large cyclic stress triggering transformation plasticity.

V. Conclusions

(1) Fatigue lifetime of 12Ce-TZP at 25° and −50°C is well correlated with the plastic strain range in low cycle fatigue, independent of the (transformation) yield stress which is lower at −50°C. The Coffin–Manson relationship in the fatigue literature of metals is applicable in this case.

(2) Fatigue failure is triggered by the propagation of preexisting process flaws, but is *preceded* by transformation-induced microcracking in the bulk. The latter strain-controlled process causes progressive degradation of flaw tolerance.

(3) Strain irreversibility is less severe in Ce-TZP than that in Mg-PSZ, probably due to some microstructural differences.

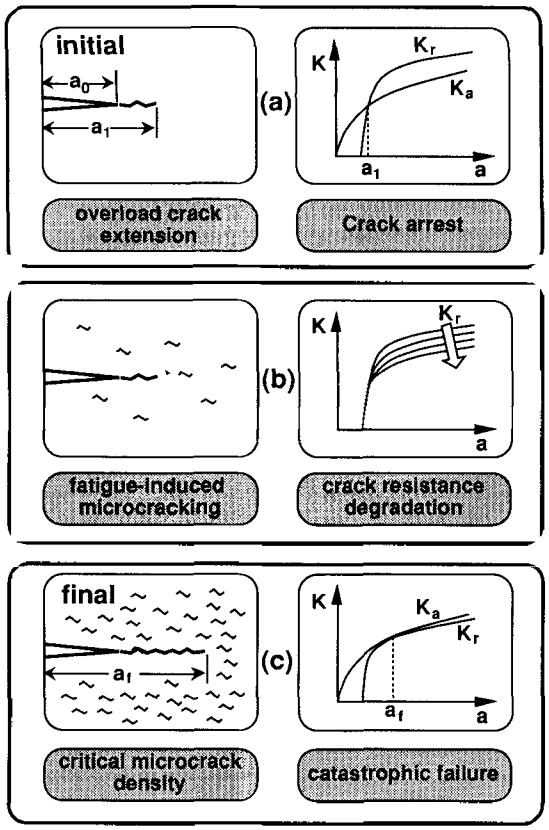

Fig. 14. Fatigue damage process in Ce-TZP.

At higher stress amplitudes and lower temperature, considerable hysteresis and strain irreversibility become more evident.

(4) No evidence for surface nucleation of fatal flaws during fatigue was found. Since Ce-TZP at low temperature has more plasticity than other strong ceramics known to date, surface nucleation in ceramics is probably unlikely.

References

[1]R. W. Hertzberg, *Deformation and Fracture Mechanics of Engineering Materials*, 3rd ed. Wiley, New York, 1989.

[2]D. A. Krohn and D. P. H. Hasselman, "Static and Cyclic Fatigue Behavior of a Polycrystalline Alumina," *J. Am. Ceram. Soc.*, **55** [4] 208–11 (1972).

[3]C. P. Chen and W. J. Knapp, "Fatigue Fracture of an Alumina Ceramic at Several Temperatures"; pp. 691–707 in *Fracture Mechanics of Ceramics 2*. Edited by R. C. Bradt, A. G. Evans, D. P. H. Hasselman, and F. F. Lange. Plenum Press, New York, 1973.

[4]R. Kossowsky, "Cyclic Fatigue of Hot-Pressed Si_3N_4," *J. Am. Ceram. Soc.*, **56** [10] 531–35 (1973).

[5]H. N. Ko, "Fatigue Strength of Sintered Al_2O_3 under Rotary Bending," *J. Mater. Sci. Lett.*, **5**, 464–66 (1986).

[6]H. N. Ko, "Cyclic Fatigue Behavior of Sintered Al_2O_3 under Rotary Bending," *J. Mater. Sci. Lett.*, **6**, 801–805 (1987).

[7]I. Maekawa, H. Shibata, and A. Kobayashi, "Bending Fatigue of Al_2O_3–ZrO_2 Ceramics," *J. Soc. Mater. Sci., Jpn.*, **36** [409] 1116–27 (1987).

[8]M. V. Swain and V. Zelizko, "Comparison of Static and Cyclic Fatigue on Mg-PSZ Alloys"; pp. 595–606 in Advances in Ceramics, Vol. 24B, *Science and Technology of Zirconia III*. Edited by S. Somiya, N. Yamamoto, and H. Hanagida. American Ceramic Society, Westerville, OH, 1988.

[9]M. Takatsu, H. Kamiya, K. Ohya, K. Ogura, and T. Kinoshita, "Effect of Vibrated Cyclic Fatigue Properties of Ceramics from Stress Load Condition," *J. Ceram. Soc., Jpn.*, **96** [10] 990–96 (1988).

[10]M. Masuda, N. Yamada, T. Soma, M. Matsui, and I. Oda, "Fatigue of Ceramics (Part 2)—Cyclic Fatigue Properties of Sintered Si_3N_4 at Room Temperature," *J. Ceram. Soc. Jpn.*, **97** [5] 520–24 (1989).

[11]M. Masuda and M. Matsui, "Fatigue in Ceramics (Part 4)—Static Fatigue Behavior of Sintered Silicon Nitride under Tensile Stress," *J. Ceram. Soc. Jpn.*, **98**, 86–95 (1990).

[12]F. Guiu, "Cyclic Fatigue of Polycrystalline Alumina in Direct Push-Pull," *J. Mater. Sci.*, **13**, 1357–61 (1978).

[13]G. Grathwohl and T. Liu, "Crack Resistance and Fatigue of Transforming Ceramics: I, Materials in the ZrO_2–Y_2O_3–Al_2O_3 System," *J. Am. Ceram. Soc.*, **74** [2] 318–25 (1991).

[14]G. Grathwohl and T. Liu, "Crack Resistance and Fatigue of Transforming Ceramics: II, CeO_2-Stabilized Tetragonal ZrO_2," *J. Am. Ceram. Soc.*, **74** [12] 3028–34 (1991).

[15]T. Kawakubo, N. Okabe, and T. Mori, "Static and Cyclic Fatigue Behavior in Ceramics"; pp. 717–26 in *Fatigue '90*, Proceedings of the Fourth International Conference on Fatigue and Fatigue Thresholds. Edited by H. Kitagawa and T. Tanaka. Materials and Component Engineering Publications Ltd., Birmingham, U.K., 1990.

[16]M. V. Swain, "Lifetime Prediction of Ceramic Materials," *Mater. Forum*, **9**, 34–44 (1986).

[17]M. Masuda, T. Soma, M. Matsui, and I. Oda, "Fatigue of Ceramics (Part 3)—Cyclic Fatigue Behavior of Sintered Si_3N_4 at High Temperature," *J. Ceram. Soc. Jpn.*, **97**, 601–607 (1989).

[18]M. Masuda, T. Soma, M. Matsui, and I. Oda, "Cyclic Fatigue of Sintered Si_3N_4," *Ceram. Eng. Sci. Proc.*, **9** [9–10] 1371–82 (1988).

[19]M. Masuda, T. Soma, and M. Matsui, "Cyclic Fatigue Behavior of Si_3N_4 Ceramics," *J. Eur. Ceram. Soc.*, **6**, 253–58 (1990).

[20]B. K. Sarkar and T. G. J. Glinn, "Fatigue Behavior of High-Al_2O_3 Ceramics," *Trans. Br. Ceram. Soc.*, **69**, 199–203 (1970).

[21]P. E. Reyes-Morel and I-W. Chen, "Transformation Plasticity of CeO_2-Stabilized Tetragonal Zirconia Polycrystals: I, Stress Assistance and Autocatalysis," *J. Am. Ceram. Soc.*, **71** [5] 343–53 (1988).

[22]P. E. Reyes-Morel, J.-S. Cherng, and I-W. Chen, "Transformation Plasticity of CeO_2-Stabilized Tetragonal Zirconia Polycrystals: II, Pseudoelasticity and Memory Effect," *J. Am. Ceram. Soc.*, **71** [8] 648–57 (1988).

[23]S.-Y. Liu and I-W. Chen, "Fatigue of Yttria-Stabilized Zirconia: I, Fatigue Damage, Fracture Origins, and Lifetime Prediction," *J. Am. Ceram. Soc.*, **74** [6] 1197–205 (1991).

[24]S.-Y. Liu and I-W. Chen, "Fatigue of Yttria-Stabilized Zirconia: II, Crack Propagation, Fatigue Striations, and Short-Crack Behavior," *J. Am. Ceram. Soc.*, **74** [6] 1206–216 (1991).

[25]S.-Y. Liu and I-W. Chen, "Fatigue Deformation Mechanisms of Zirconia Ceramics," *J. Am. Ceram. Soc.*, **75** [5] 1191–204 (1992).

[26]I-W. Chen and P. E. Reyes-Morel, "Transformation Plasticity and Transformation Toughening in Mg-PSZ and Ce-TZP"; pp. 75–88 in Materials Research Society Symposia Proceedings, Vol. 78, *Advanced Structural Ceramics*. Edited by P. F. Becher, M. V. Swain, and S. Somiya. Elsevier, New York, 1987.

[27]K. Tsukuma and T. Takahata, "Mechanical Property and Microstructure of TZP and TZP/Al_2O_3 Composites"; pp. 123–35 in Materials Research Society Symposia Proceedings, Vol. 78, *Advanced Structural Ceramics*. Edited by P. F. Becher, M. V. Swain, and S. Somiya. Elsevier, New York, 1987.

[28]ASTM Standard E.606-80, "Standard Recommended Practice for Constant-Amplitude Low Cycle Fatigue Testing"; pp. 652–69 in *ASTM Annual Book of Standards 3.01*. American Society for Testing and Materials, Philadelphia, PA, 1983.

[29]P. E. Reyes-Morel and I-W. Chen, "Stress-Biased Anisotropic Microcracking in Zirconia Polycrystals," *J. Am. Ceram. Soc.*, **73** [4] 1026–33 (1990).

[30]I-W. Chen and P. E. Reyes-Morel, "Implication of Transformation and Plasticity in ZrO_2-Containing Ceramics: I, Shear and Dilatation Effects," *J. Am. Ceram. Soc.*, **69** [3] 181–89 (1986). □